Cellular and Molecular Life Sciences (2023) 80:165
https://doi.org/10.1007/s00018-023-04810-y

ORIGINAL ARTICLE

G6PD activation in TNBC cells induces macrophage recruitment and M2 polarization to promote tumor progression

Yin Li[1] · Xiao Han[1] · Zhoujun Lin[1] · Changjun Wang[3] · Zhenkun Fu[2] · Qiang Sun[3] · Chenggang Li[1]

Received: 13 February 2023 / Revised: 28 April 2023 / Accepted: 16 May 2023 / Published online: 27 May 2023

Abstract

Glucose-6-phosphate dehydrogenase (G6PD) is involved in triple-negative breast cancer (TNBC) progression. Metabolic crosstalk between cancer cells and tumor-associated macrophages mediates tumor progression in TNBC. Molecular biological methods were applied to clarify the mechanism of the crosstalk between TNBC cells and M2 macrophages. In the present study, we verified that G6PD overexpression drives M2 macrophage polarization by directly combining with phospho-STAT1 and upregulating CCL2 and TGF-β1 secretion in TNBC cells. In turn, M2-like TAMs activated TNBC cells through IL-10 secretion, providing feedback to upregulate G6PD and promote TNBC cell migration and proliferation in vitro. Furthermore, we found that 6-AN (a specific inhibitor of G6PD) not only suppressed the cancer-driven polarization of macrophages toward the M2 phenotype but also inhibited the inherent M2 polarization of macrophages. Targeting the G6PD-regulated pentose phosphate pathway restrained TNBC progression and M2-type polarization of macrophages in vitro and in vivo.

Keywords TNBC · G6PD · 6-AN · M2 macrophages

Abbreviations

TNBC	Triple-negative breast cancer.
PPP	Pentose phosphate pathway.
G6PD	Glucose-6-phosphate dehydrogenase.
6-AN	6-Aminonicotinamide.
TAMs	Tumor-associated macrophages.
Mφ	Macrophage.
ELISA	Enzyme-linked Immunosorbent Assay.
CM	Conditioned medium.
q-PCR	Quantitative polymerase chain reaction.
MTT	Thiazolyl blue.
IHC	Immunohistochemistry.
H&E	Hematoxylin and eosin.
DAPI	4′,6-Diamidino-2-phenylindole.
CCL2	Chemokine (C–C motif) ligand 2
TGF-β1	Transforming growth factor beta 1
IL-10	Interleukin-10

✉ Changjun Wang
wangchangjun@pumch.cn

✉ Zhenkun Fu
300042@hrbmu.edu.cn

✉ Qiang Sun
sunqiangpumch@sina.com

✉ Chenggang Li
lichenggang@nankai.edu.cn

[1] State Key Laboratory of Medicinal Chemical Biology and College of Pharmacy, Nankai University, No.38 Tongyan Road, Jinnan District, Tianjin 300350, People's Republic of China

[2] Department of Immunology, Wu Lien-Teh Institute, Heilongjiang Provincial Key Laboratory for Infection and Immunity, Harbin Medical University & Heilongjiang Academy of Medical Science, No.157 Baojian Street, Nangang District, Harbin 150086, People's Republic of China

[3] Department of Breast Surgery, Peking Union Medical College Hospital, No.1 Shuaifuyuan, Dongcheng District, Beijing 100730, China

Introduction

Among the most common cancers diagnosed in women in 2021, breast cancer alone accounted for 30% of female cancers. Breast cancer has the highest incidence among all female malignancies and remains one of the leading causes of cancer-related death [1]. Currently, the concept of intrinsic subtype is widely recognized and used for breast cancer treatment guidance. Among different subtypes, triple-negative breast cancer (TNBC) is defined as lacking estrogen receptor (ER), progesterone receptor (PR), and human epidermal growth factor receptor 2 (HER2) expression and

accounts for approximately 20% of all breast cancer subtypes [2]. Compared to other molecular subtypes, TNBC exhibits more powerful invasiveness, a higher recurrence rate and a worse prognosis. Due to the lack of specific therapeutic targets, the TNBC mortality rate is stubbornly high and remains a huge challenge for oncologists.

Recently, energy metabolism reprogramming has been recognized as one of the hallmark events that contributes to carcinogenesis. TNBC has a unique energy metabolism model, and it is much more dependent on glucose metabolism than non-TNBC (MCF-7) [3]. In glucose catabolism, the pentose phosphate pathway (PPP) is one of the major pathways. The PPP directly or indirectly provides reducing power to fuel the biosynthesis of lipids and nucleotides and sustains antioxidant responses to support cell survival and proliferation. In the PPP, glucose-6-phosphate dehydrogenase (G6PD) is the rate-limiting enzyme and acts as a "gatekeeper" of this pathway. The activity of G6PD directly reflects the flux of the PPP. Previous studies revealed that G6PD was highly dependent on the breast cancer molecular subtype, and its overexpression was associated with poor prognosis [4, 5].

No disease exists on its own, and breast cancer is no exception. Its carcinogenesis involves the tumor microenvironment (TME). The TME is a dynamic entity composed of cancerous and noncancerous cells. Macrophages are the most abundant infiltrating immune cells present in and around tumors, and they can be polarized into classically activated M1-type macrophages or alternately activated M2-type macrophages by different stimuli. An important feature of macrophages is that they can rapidly change their activation status and function in response to microenvironment signals. In the early stage of tumorigenesis, macrophages promote inflammation, whereas they become immunosuppressive in the later stage, suggesting the high plasticity of macrophages. Tumor-associated macrophages (TAMs), accounting for 50–80% of interstitial cells, have been generally considered M2-polarized TAMs [6]. To date, it is clear that TAMs exert multiple protumorigenic roles, including stimulation of angiogenesis, extracellular matrix remodeling, promotion of tumor cell survival, proliferation, invasion and metastasis, and inhibition of antitumor immunity [7]. TAMs can highly express key molecules that promote tumor cell growth and migration and play an important role in TNBC initiation, growth, and metastasis. Recently, in a coculture study of TNBC and macrophages, Gpr132 sensed lactate in the TME to transform macrophages into M2-like phenotypes to promote tumor adhesion, migration, and invasion [8]. In addition, HIF-1α-stabilizing HISLA is transferred from TAMs to TNBC via extracellular vesicle transmission, which increases glycolysis in TNBC [9]. Metabolic reprogramming in cancer cells can not only affect other cells in the TME but also contribute to the regulation of critical cancer-related processes. TAMs are influenced by their surroundings and readily respond to perturbations by altering the metabolic profile. Therefore, investigating the metabolic interactions between cancer cells and TAMs in the TME may reveal the key point of TNBC development and open new scenarios from both diagnostic and therapeutic points of view.

Our previous studies have shown that inhibition of G6PD in breast cancer cells could weaken cell viability, inhibit proliferation, and decrease migration and colony formation by inducing cell autophagic death [10]. Further studies discovered that regulating G6PD in TNBC affected the transformation of macrophages into TAMs. In the present study, we found that suppression of G6PD altered cytokine secretion in TNBC, thereby inhibiting macrophage polarization toward the M2 phenotype. On the other hand, M2 macrophages exhibited activation of the PPP. G6PD inhibitors prevented M2 polarization of macrophages and inhibited the pro-oncogenic effect of M2 macrophages. This work revealed that targeting G6PD inhibited TNBC survival and metastasis by triggering a positive feedback loop between macrophages and cancer cells. G6PD may be a promising therapeutic target for TNBC.

Materials and methods

Cell lines and culture

The human breast cancer cell lines MDA-MB-231 (MDA-231), MDA-MB-453 (MDA-453), MDA-MB-468 (MDA-468), MCF10A and THP-1 were purchased from ATCC. THP-1 cells were cultured in RPMI 1640 medium with 10% FBS and 100U/mL penicillin/0.1 mg/mL streptomycin (1% penicillin/streptomycin). MDA-231, MDA-453 and MDA-468 cells were cultured in Dulbecco's modified Eagle's medium (DMEM) with 10% FBS and 1% penicillin/streptomycin. MCF10A cells were grown in DMEM F-12 supplemented with 5% horse serum, 10 μg/mL human insulin, 20 ng/mL EGF, 100 ng/mL cholera toxin, 0.5 μg/mL hydrocortisone, and 1% penicillin/streptomycin. MDA-MB-231 shNC/shG6PD cells were established in our lab and cultured in the corresponding medium with 10% FBS, 1% penicillin/streptomycin and 1 μg/mL puromycin. All cultures were incubated at 37 °C in a humidified 5% CO_2 atmosphere. Phorbol-12-myristate-13-acetate (PMA) was purchased from Beyotime. THP-1 cells were treated with PMA (100 ng/mL) for 24 h to differentiate the cells into resting macrophages (M0 cells). The M2 phenotype was generated using 30 ng/mL IL-4 (PeproTech, Rocky Hill, NJ, USA) stimulation for 48 h. The M1 phenotype was generated using 50 ng/mL

IFNγ (PeproTech, Rocky Hill, NJ, USA) and 300 ng/mL LPS (Beyotime, Shanghai, China) stimulation for 48 h.

Conditioned medium preparation

Cells were seeded in 6-well or 10 cm plates at a density of 70% cells in serum-containing medium. After cell attachment, the medium was replaced with serum-free medium, and the cells were incubated for an additional 24 h/48 h. The conditioned medium was collected and centrifuged at 3000 rpm for 5 min to remove the cells or cell debris.

Cytokine array analysis

Cells were seeded in 10 cm plates (1×10^6 cells/plate) with serum-free medium for 48 h. The conditioned medium (CM) was centrifuged for 5 min at 3000 rpm, and then the supernatant was collected to perform the assay. Human Cytokine Antibody Array C5 (RayBiotech, Peachtree Corners, Georgia, USA) was incubated overnight with 3 mL of CM at 4 °C. After washing with the buffer, the membranes were incubated for 2 h at room temperature with biotinylated antibody cocktail, washed three times, reacted with HRP-streptavidin in blocking buffer for 2 h at room temperature and photographed on a chemiluminescence imaging system.

ELISA

Cytokine secretion in the culture medium was assayed using an ELISA kit according to the manufacturer's protocol, CCL2 and IL-10 (mlbio, Shanghai, China), TGF-β1 and IFNγ (Jiangsu Meimian Industrial Co., Ltd, Jiangsu, China). Human recombinant CCL2, TGF-β1 and IL-10 were purchased from PeproTech (Rocky Hill, NJ, USA). Intracellular levels of Ru-5-P was assayed using an ELISA kit according to the manufacturer's protocol.

G6PD activity assay

G6PD activity was measured in cells using a Beyotime kit (G6PDH Activity Assay Kit with WST-8, Shanghai, China) according to the manufacturer's instructions. Values were normalized to the protein content in each sample.

NADPH level assay

NADPH level was detected using Beyotime kit (NADP+/NADPH Activity Assay Kit with WST-8, Shanghai, China) according to the manufacturer's instructions.

Western blot analysis

The primary antibodies used in this study were CD163 (Abcam, Cambridge, UK), CD80 and CD86 (Bioss, Boston, MA, USA), 6PGD (Sigma, Burlington, MA, USA), phospho-STAT1 (Ser727), phospho-NFκB p65 (Ser536), G6PD, PKM2, HK2, GLUT1 and GLUT4 (Cell Signaling Technologies, Danvers, MA, USA), CD206, phospho-STAT3 (Tyr705), STAT3, STAT1, NFκB p65, GLUT3, Lamin B1 and β-actin (Santa Cruz, Dallas, Texas, USA). α-tubulin (Neomarker, Fremont, CA, USA). The blotted membranes were then scanned using Tanon 5200 Multi acquisition software.

Cell viability assay

Change in suspension cell viability was determined by using the Cell Counting Kit-8 (CCK-8; MeilunBio, Dalian, China) assay. THP-1 cells were seeded into 96-well plates in 200 μL of the tumor conditioned medium and incubated for additional 24 h at 37 °C. At the end of each experiment, CCK8 reagent was added to the cells (20 μL per well) and the cells were further cultured for 2 h at 37 °C to measure cell viability. The absorbance was measured at OD = 450 nm.

The MTT assay was carried out to determine cell viability. Briefly, 20 μL of MTT solution (5 mg/mL) was added to each well. After incubation for 1–4 h, 100 μL of DMSO was added to each well and cultured at 37 °C for 10 min. The absorbance was measured at OD = 490 nm.

Chromatin immunoprecipitation (ChIP) assay

ChIP was presented using ChIP kit (absin, Shanghai, China). The cells were cultured in 10 cm petri dishes and operated according to the manufacturer's instructions. The samples were immunoprecipitated with phospho-STAT1 and IgG antibodies. Complexes of DNA and protein were pulled down by phospho-STAT1 antibodies, IgG antibody was set as a negative control. Primers for the amplification containing phospho-STAT1-binding site-specific region of CCL2 promoter (nucleotides − 376 bp to − 79 bp) were designed as forward 5′-GGAATGTGGCCTGAAGGT-3′ and reversed 5′-TGATAAGTGGGCTGTTAAATC-3′, and the size of production was expected to 298 bp. STAT1 binding motif (nucleotides − 717 bp to − 382 bp) in TGF-β1 promoter sequences was designed as forward 5′-TGGCACAGTGGT CAAGAGC-3′ and reversed 5′-CTGGGAAACAAGGTA GGAGAAG-3′, and the size of production was expected to 336 bp. PCR was presented to amplify the sequence of the target gene.

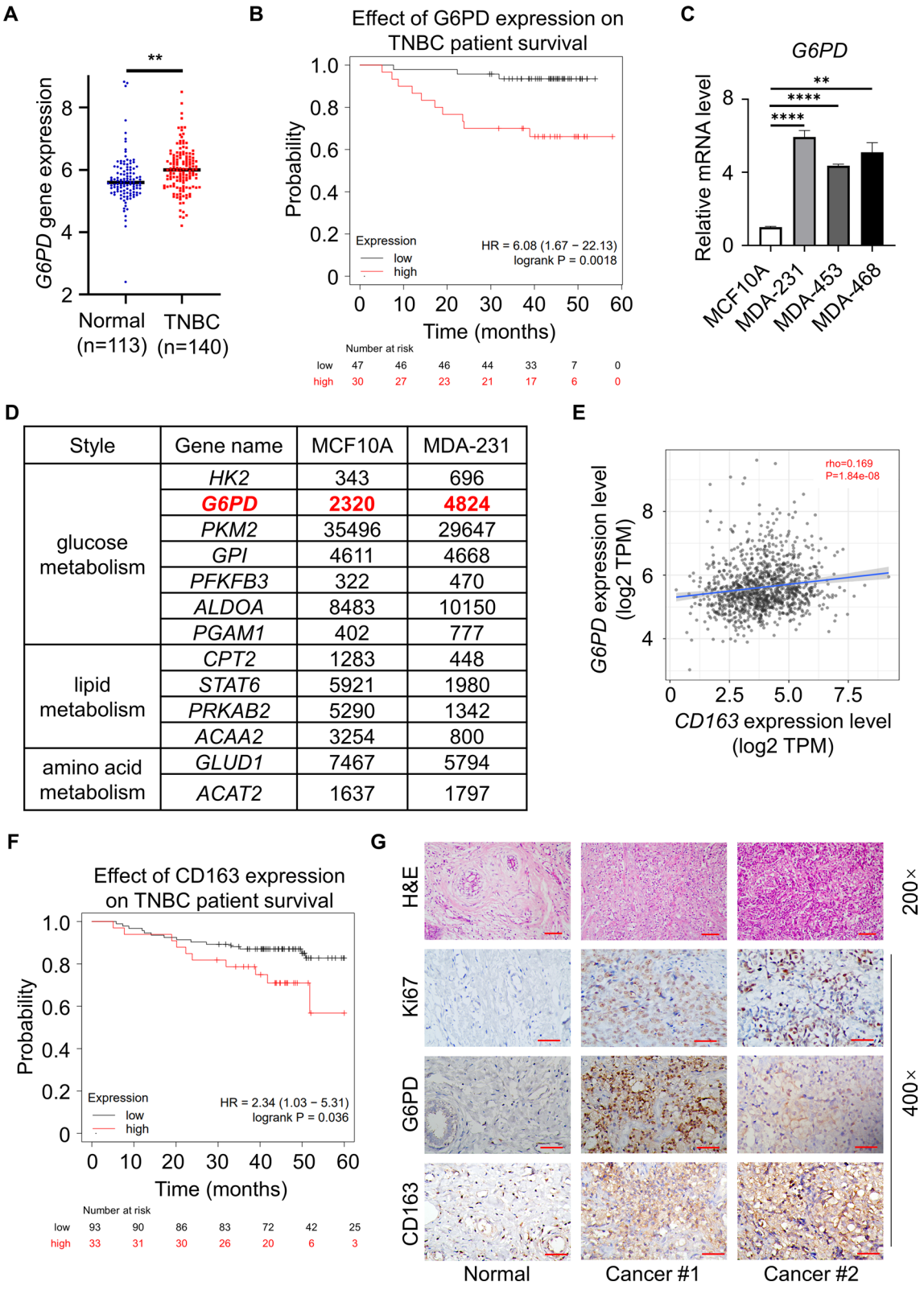

Style	Gene name	MCF10A	MDA-231
glucose metabolism	*HK2*	343	696
	G6PD	**2320**	**4824**
	PKM2	35496	29647
	GPI	4611	4668
	PFKFB3	322	470
	ALDOA	8483	10150
	PGAM1	402	777
lipid metabolism	*CPT2*	1283	448
	STAT6	5921	1980
	PRKAB2	5290	1342
	ACAA2	3254	800
amino acid metabolism	*GLUD1*	7467	5794
	ACAT2	1637	1797

◂**Fig. 1** Correlation of G6PD expression in TNBC and TAM infiltration. **A** The TCGA database was used to analyze the gene expression of *G6PD* in normal individuals ($n=113$) and TNBC patients ($n=140$). **B** The Kaplan−Meier Plotter website was used to investigate the relationship between G6PD expression and survival probability in TNBC human samples (n(high) = 30, n(low) = 47). **C** q-PCR analysis of the transcription levels of *G6PD* in TNBC compared to MCF10A cells. **D** Reanalysis of previously published expression array data (GEO accession number GSE81032) was performed using an online tool. **E** Statistical analysis revealed that the expression intensity of G6PD was positively correlated with CD163. **F** The Kaplan−Meier Plotter website was used to investigate the relationship between CD163 infiltration and survival probability in TNBC human samples (n(high) = 33, n(low) = 93). **G** IHC staining detected G6PD, CD163 and Ki67 in human breast cancer tissues and adjacent normal tissues. TNBC patient tissue sections were collected from the hospital (Magnification 400×, bar = 50 μm. Magnification 200×, bar = 100 μm). $^{**}P<0.01$, $^{****}P<0.0001$

Co-immunoprecipitation (Co-IP) assay

Measures of 1 μg of anti-G6PD and anti-phospho-STAT1 antibodies were incubated with cell lysate after different treatments for 4 h at 4 °C, followed by incubation with protein-A/G agarose (Santa Cruz Biotechnology, Texas, USA) overnight at 4 °C. The beads were washed 5 times and suspended with SDS loading buffer, then centrifuged after boiling to acquire the supernatant for immunoblotting analysis.

Nuclear and cytosolic extractions

Extracts of cytosolic and nuclear were isolated by using the nuclear and cytoplasmic extraction kit (Solarbio, Peking, China) according to the manufacturer's recommendations.

Flow cytometry staining

Cells were centrifuged at 1000 rpm for 5 min, washed with PBS and filtered through a 100-μm mesh. The cells were subsequently stained with an antibody against an M2 macrophage surface markers (PE-labeled anti-human CD163 (Biolegend, CA, USA)). All data were collected using BD LSR Fortessa flow cytometer (BD Biosciences, NJ, USA) and analyzed using FlowJo software (BD Biosciences, NJ, USA).

Immunohistochemistry (IHC)

IHC analysis was carried out to test G6PD, CD163 and Ki67 expression profiles in tissues. The primary antibodies were applied to the slides and incubated at 4 °C overnight. The slides were washed and then stained with the secondary antibody and DAB.

Cell migration assay

Cancer cells (1×10^5) were seeded into the upper chamber in 200 μL of serum-free medium and cocultured with M0/M2-Mφ (5×10^5) in the bottom chamber in 750 μL of 20% FBS medium.

In addition, a total of $8–10\times10^4$ cells per well were seeded in the upper chamber in 200 μL of serum-free medium or serum-free medium containing IL-10, IL-10R Ab (R&D Systems, Minneapolis, Minnesota, USA) or TGF-β1, and 750 μL of 20% FBS medium was added to the lower chamber. After incubation at 37 °C for another 24 h or 48 h, the cells remaining at the upper surface of the membrane were removed with cotton swabs, and the cells on the lower surface of the membrane were the migrated cells. The cells were fixed in 10% formalin for 10 min and then stained with 0.05% crystal violet for 10 min.

EdU cell proliferation assay

Cells were seeded in a 24-well culture plate at a rate of 6×10^4 cells/well and incubated for 48 h. An EdU analysis kit (Beyotime) was used to analyze and evaluate cell proliferation, and the specific method was carried out following the instructions provided by the manufacturer. The samples were analyzed with a confocal microscope (Leica).

q-PCR

Total RNA was extracted using TRIzol (Thermo Fisher Scientific, Waltham, MA, USA) according to the manufacturer's instructions. Then, 1 μg of RNA from each sample was reverse transcribed to cDNA by the First Strand cDNA Synthesis Kit (YEASEN, Shanghai, China). q-PCR was performed using SuperReal PreMix Plus SYBR Green (TIANGEN, Beijing, China) in a final volume of 10 μL on a PCR machine. The primer pairs for human genes were as follows:

***G6PD*,**

F: CGAGGCCGTCACCAAGAAC, R: GTAGTGGTCGATGCGGTAGA.*β-actin*,

F: CACCATTGGCAATGAGCGGTTC, R: AGGTCTTTGCGGATGTCCACGT.

CCL2,

F: CAGCCAGATGCAATCAATGCC, R: TGGAATCCTGAACCCACTTCT.

TGF-β1,

F: CTAATGGTGGAAACCCACAACG, R: TATCGCCAGGAATTGTTGCTG.

IL-10,

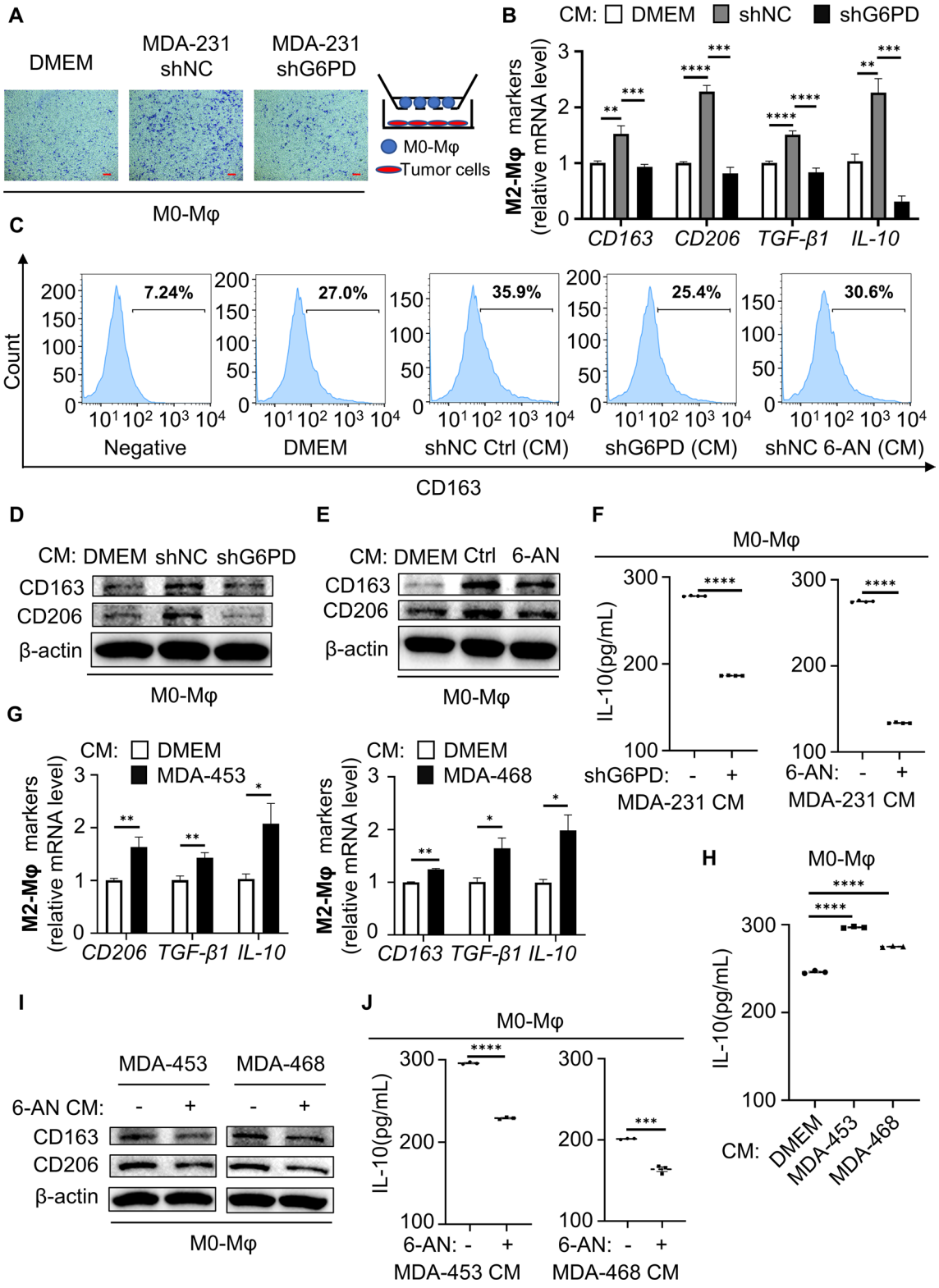

F: GACTTTAAGGGTTACCTGGGTTG, R: TCACATGCGCCTTGATGTCTG.

CD206,

F: TCCGGGTGCTGTTCTCCTA, R: CCAGTCTGTTTTTGATGGCACT.

CD163,

◂**Fig. 2** G6PD expressed in TNBC cells induced macrophage recruitment and M2 polarization in vitro. **A** Transwell migration assays used M0-Mφ cells in the upper chamber and tumor cells in the lower chamber. **B** Levels of the M2 markers were compared by q-PCR after M0-Mφ coculture with the specified MDA-231-CM for 6 h. **C** Flow cytometry was used to measure the amount of CD163 positive in macrophages. **D**, **E** The protein expression was determined using western blotting after M0-Mφ coculture with the specified MDA-231-CM for 6 h. **F** ELISA measured the secretion of the M2-polarizing cytokine IL-10 in macrophages cocultured with the specified CM. **G** Gene expression was measured using q-PCR after M0-Mφ coculture with the indicated CM for 6 h. **H** IL-10 secretion in M0-Mφ cocultured with the indicated CM was analyzed by ELISA. **I** Immunoblot analysis of protein expression after M0-Mφ coculture with the specified CM for 6 h. **J** ELISA measured IL-10 after M0-Mφ coculture with the specified CM. **F**, **H**, **J** CM was added to M0-Mφ for 6 h and replaced with serum-free culture for 6 h. The supernatants were recovered and analyzed for IL-10 secretion. $*P<0.05$, $**P<0.01$, $***P<0.001$, $****P<0.0001$

F: TTTGTCAACTTGAGTCCCTTCAC, R: TCCCGCTACACTTGTTTTCAC.

CD86,

F: CTGCTCATCTATACACGGTTACC, R: GGAAACGTCGTACAGTTCTGTG.

IL-1β,

F: ATGATGGCTTATTACAGTGGCAA, R: GTCGGAGATTCGTAGCTGGA.

IL-12,

F: GTCGGAGATTCGTAGCTGGA, R: CCATGACCTCAATGGGCAGAC.

M-CSF,

F: AGACCTCGTGCCAAATTACATT, R: AGGTGTCTCATAGAAAGTTCGGA.

TNF-α,

F: GAGGCCAAGCCCTGGTATG, R: CGGGCCGATTGATCTCAGC.

TIMP2,

F: GCTGCGAGTGCAAGATCAC, R: TGGTGCCCGTTGATGTTCTTC.

IGFBP2,

F: GACAATGGCGATGACCACTCA, R: CAGCTCCTTCATACCCGACTT.

IFNγ,

F: GAGGCCAAGCCCTGGTATG, R: CGGGCCGATTGATCTCAGC.

STAT1

F: CAGCTTGACTCAAAATTCCTGGA, R: TGAAGATTACGCTTGCTTTTCCT

Xenografted tumor model

Specific pathogen-free (SPF) 5-week-old female CD-1 nude mice were used in this study and maintained in accordance with institutional guidelines for the use of laboratory animals. MDA-MB-231 cells (5×10^6 cells in 100 μL of PBS) bearing a luciferase reporter were injected subcutaneously into the bilateral mammary glands of nude mice. The survival time of differentiated macrophages in vivo is generally approximately 20 days. Therefore, we first inoculated MDA-MB-231 cells subcutaneously into mice, and when the tumor volume reached approximately 250 mm^3, we inoculated 3×10^5 THP-1 cells treated with PMA (M0) macrophages around the tumor.

Luminescent tumor images were checked weekly after the intraperitoneal injection of luciferin (150 mg/kg) (PerkinElmer) and assessed using bioluminescence imaging (BLI). Images were analyzed by Living Image Software 4.5 through the photon flux of the BLI signal within a region. Tumor volumes were calculated by the formula V (mm^3) = (Length * $width^2$)/2. The primary tumor tissue was removed. Five mice were included in each group. After 3 weeks, the mice were euthanized, and the tumors were dissected and prepared for protein or RNA extraction. Tissues were fixed in 4% formaldehyde and prepared for histopathological evaluation.

Statistical analysis

All experiments were repeated at least three independent times. Statistical analysis was performed using GraphPad Prism software. Data are presented as the means ± S.E.M. Statistical differences between the two groups were analyzed using Student's t test. $p<0.05$ was considered a statistically significant difference.

Result

Correlation of G6PD expression in TNBC and TAM infiltration

Recently, metabolic reprogramming has emerged as a hallmark of cancer cells, and these alterations confer many advantages to cancer cells, including the promotion of biosynthesis, ATP generation, detoxification and support of rapid proliferation. TNBC, which is a high-grade breast cancer, is especially dependent on glucose metabolism, particularly the PPP. Because G6PD acts as a "gatekeeper" of the PPP, the activity of G6PD directly reflects the PPP flux. We detected overexpression of *G6PD* in TNBC patients relative to normal breast tissues (Figs. 1A and S1A). Meanwhile, we observed that high G6PD expression in patients was associated with a lower survival probability in the TNBC subtype (Fig. 1B). To further determine G6PD expression in TNBC (MDA-231, MDA-453 and MDA-468), q-PCR and immunoblot analysis were performed in TNBC cells. The results

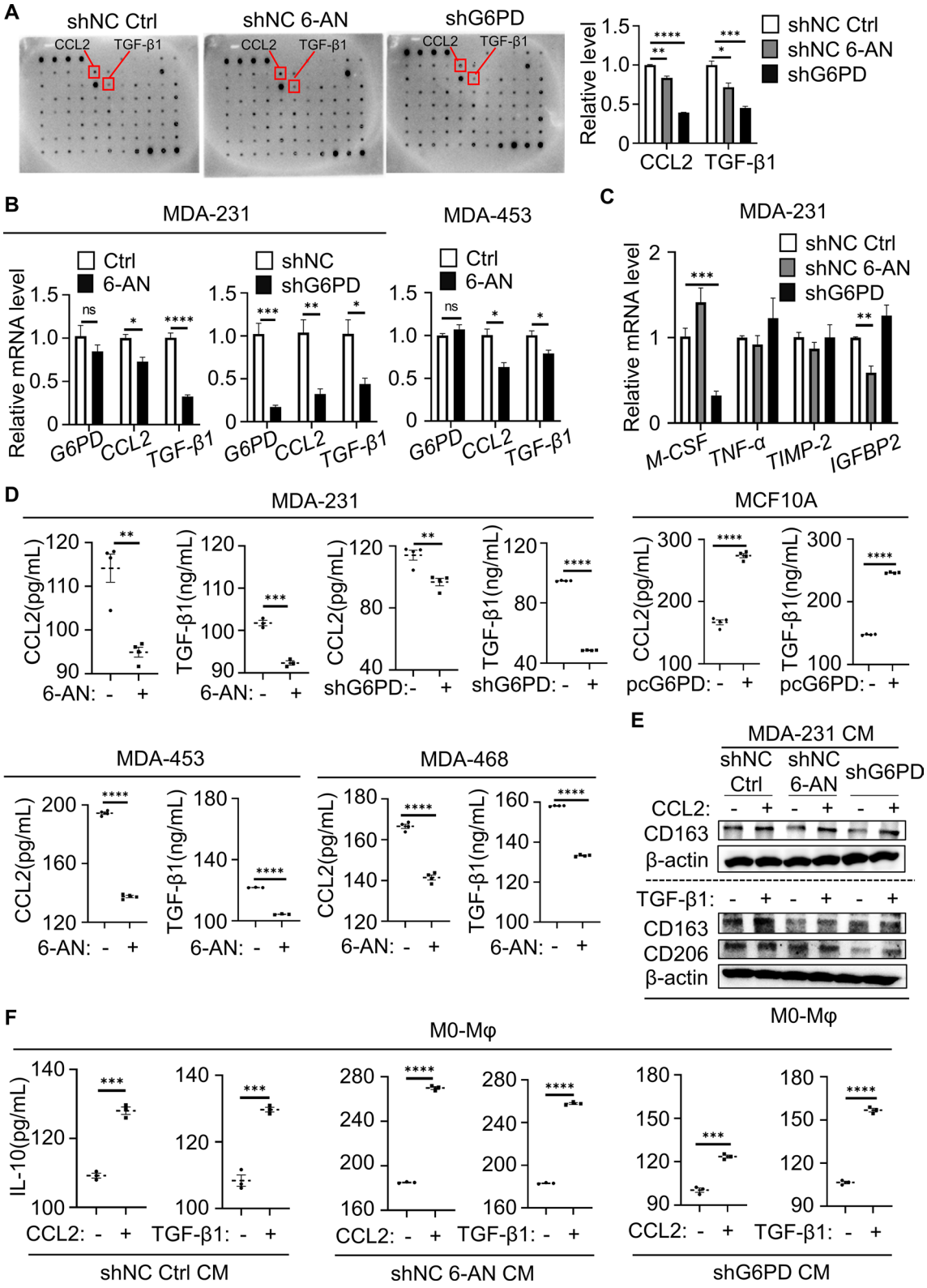

showed that the expression of G6PD was upregulated at both the transcriptional and translational levels in TNBC cells compared with normal breast epithelial MCF10A cells (FigS. 1C and S1B). By analyzing the key molecules of glycometabolism, lipid metabolism and amino acid metabolism in public gene databases [11], *G6PD*

◂**Fig. 3** G6PD-triggered cytokine secretion contributed to M2-Mφ activation. **A** Cytokine arrays were incubated with the CM of MDA-231 cells (shNC control vs. shNC 6-AN (20 μM) vs. shG6PD) to identify the secreted cytokines specific to the indicated cellular conditions. The right graph summarizing the relative levels of the indicated cytokines is presented. The red box indicates the site of CCL2 and TGF-β1. **B** Gene expression of *G6PD*, *CCL2* and *TGF-β1* was measured using q-PCR. Cells were treated with 6-AN for 24 h. **C** MDA-231 cells were treated with 6-AN for 24 h. The mRNA levels of *M-CSF*, *TNF-α*, *TIMP-2* and *IGFBP2* were detected by q-PCR. **D** CCL2 and TGF-β1 contents in the CM of MDA-231, MDA-453, MDA-468 or MCF10A cells as determined by ELISA. **E** Immunoblotting analysis of CD163 and CD206 levels in M0-Mφ cocultured with MDA-231-CM after the addition of 30 ng/mL CCL2 or TGF-β1 to the coculture system. **F** ELISA detected levels of IL-10 in CM from M0-Mφ cocultured with MDA-231-CM after the addition of 30 ng/mL CCL2 or TGF-β1 to the coculture system. **E**, **F** CM was added to M0-Mφ for 6 h and replaced with serum-free culture for 6 h. The cells were harvested, and the supernatants were recovered. **A**–**F** TNBC cells were treated with 6-AN (20 μM for MDA-231, 50 μM for MDA-453 and MDA-468). $^{*}P<0.05$, $^{**}P<0.01$, $^{***}P<0.001$, $^{****}P<0.0001$

expression was found to be upregulated significantly in MDA-231 cells compared with MCF10A cells (Fig. 1D). After that, we linked G6PD expression with clinical data from the patients and found that G6PD expression was associated with patient's race. In Asian, there are more breast cancer patients with high expression of G6PD in tumor cells. However, there was no association of G6PD between the different N stage, cancer stages and age of the patients (Fig. S1C–F). The abovementioned results suggested that the expression of G6PD was upregulated both in human TNBC cells and tissues.

The choice and extent of metabolic reprogramming directly met the survival need of tumors and promoted tumor development by altering the function of noncancerous cells in the metabolic crosstalk of the surrounding microenvironment [12]. Notably, immune cells were the largest population in non-cancerous cells, in particular tumor associated macrophages (TAMs). Thus, we analyzed the expression of G6PD with CD163 (a specific marker for M2-Mφ), results showed that G6PD was positively correlated with CD163 in TIMER database (http://timer.cistrome.org/) (Fig. 1E), and higher expression of CD163 indicated poorer prognosis (Fig. 1F). To evaluate G6PD and CD163 expression and relationship in human TNBC tissues, the levels of these protein expression were detected in TNBC fresh tissues and matched adjacent normal (Non-TNBC) tissues by IHC. IHC confirmed that the tumor samples showed a higher G6PD and CD163 than adjacent normal samples (Fig. 1G). Above all, the link between G6PD and TAM infiltration may have important implications in the study of TNBC.

G6PD expressed in TNBC cells induced macrophage recruitment and M2 polarization in vitro.

Macrophages differentiate into two polarization types, M1 and M2. In the tumor microenvironment, TAMs often exhibit M2 polarization and are associated with malignant transformation of tumor cells and poor prognosis of patients [13]. Theoretically, G6PD overexpression in TNBC cells may impact not only cancer cells but also macrophages. We employed the human THP-1 monocyte–macrophage differentiation model. Treatment THP-1 cells with PMA for 24 h results in differentiated macrophage cells (M0-Mφ) displaying an adherent phenotype with extended pseudopods. Firstly, to investigate the impact of the activation of G6PD in tumor cell on macrophage proliferation and migration, we examined the effect of the G6PD expression in tumor cell on macrophage migration in transwells co-culture system. In co-culture assays, G6PD-deficient tumor cells were seeded at lower chamber, and M0-Mφ were implanted in the upper chamber. After 48 h, migrated macrophages were stained and counted. We found that control cells promoted macrophage migration by fourfold, whereas G6PD knockdown cells abrogated the induction of macrophage migration (Fig. 2A and S2A). We then examined the roles of G6PD in tumor cell on macrophage proliferation, THP-1 cells were treated with the conditioned media (CM) from control and G6PD knockdown cells. CCK-8 assays showed that CM from control cells promoted THP-1 proliferation, whereas CM from G6PD knockdown cells abolished the induction of THP-1 proliferation (Fig. S2B). Meanwhile, the TIMER database revealed the expression of G6PD correlated positively with CD68 (a specific marker for macrophage) in breast cancer (Fig. S2C). These results indicated that G6PD promoted macrophages recruitment in the TME of TNBC. Next, we wondered whether tumor cell-expressed G6PD modulated macrophage polarization by treating macrophages with tumor-CM. Specifically, we tested the influence of CM from TNBC cells on the polarization of macrophages. TNBC cells CM was cultured in serum-free medium for 48 h and added to M0 macrophages for 6 h to identify markers of M1-Mφ and M2-Mφ. Interestingly, the induced mRNA levels of M2-Mφ markers (*CD163*, *CD206*, *IL-10* and *TGF-β1*) were relatively increased in macrophages cocultured with CM from MDA-231 cells compared with DMEM, but the increase was significantly impaired upon shRNA-mediated knockdown of G6PD. However, there was no difference in M1-related markers (*CD86*, *IL-12* and *IL-1β*) in human macrophages (Figs. 2B and S2D). The M2 macrophages surface markers CD163 was measured by flow cytometry. Increased ratio of CD163 in macrophages were observed with the CM of control MDA-231 cells treatment,

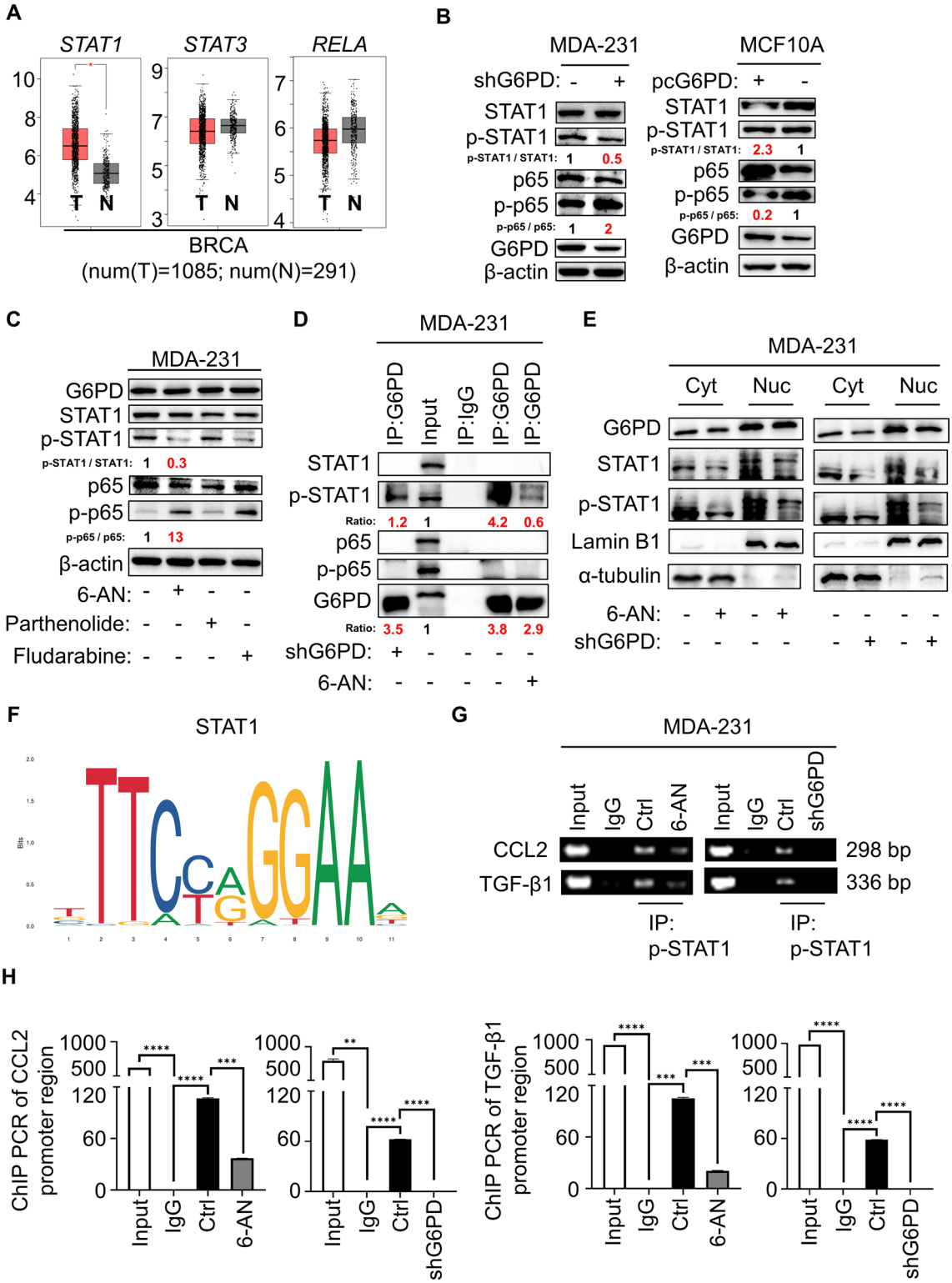

and the percentage of CD163 positive cells was lower in macrophages cocultured with the CM of cells with G6PD knockdown or 6-aminonicotinamide (6-AN, a specific inhibitor of G6PD) (Figs. 2C and S2E). Consistently, both the CM of cells with G6PD knockdown and 6-AN treatment reduced CD163 and CD206 protein abundance in macrophages (Figs. 2D,E). These results indicated that G6PD deficiency inhibited the polarization of M2-like macrophages in the TME. Then, G6PD was overexpressed in MCF10A cells, accompanied with increased protein expression and activity

◂**Fig. 4** G6PD-controlled cytokine secretion achieved by STAT1 signaling. **A** The StarBase 3.0 website examined the gene expression of *STAT1*, *STAT3*, and *RELA* in healthy persons ($n=291$) and breast cancer patients ($n=1085$). **B** Immunoblot analysis of the proteins in MDA-231-shG6PD, MCF10A-pcG6PD and corresponding control cells. **C** MDA-231 cells were treated with 6-AN, parthenolide or fludarabine. The levels of proteins were assessed by immunoblotting. **D** MDA-231 cells were harvested and subjected to immunoprecipitation with anti-G6PD, followed by Western blot analysis with the indicated antibodies. **E** Western blot analysis was used to detect indicated proteins from the cytosolic and nuclear extracts. **F** Schematic diagram showing the potential binding sites in the promoter region for STAT1. **G**, **H** q-PCR was performed to determine gene abundance of CCL2 or TGF-β1 promoter region in the groups of positive control (Input), negative control (IgG) and IP, which were immunoprecipitated with anti- phospho-STAT1 antibody in MDA-231 cells (G) and statistically analyzed (H). $*P<0.05$, $**P<0.01$, $***P<0.001$, $****P<0.0001$

(Fig. S2F and S2G). CM was added to M0-Mφ for 6 h and then incubated in serum-free medium for 6 h. The supernatants were recovered and analyzed for IL-10 secretion by ELISA. Consistently, it was demonstrated that IL-10 was increased in the supernatants of macrophages co-incubated with CM from G6PD-overexpressing MCF10A cells, and this IL-10 increasement could be reversed by G6PD inhibition (Figs. 2F and S2H). Moreover, other TNBC cell lines, such as MDA-435 and MDA-468, also showed a similar effect of G6PD on the M2 polarization of macrophages (Fig. 2G–J). Taken together, G6PD-induced macrophage M2 polarization is common in TNBC and is worthy of further investigation.

G6PD-triggered cytokine secretion contributed to M2-Mφ activation

Cell−cell interactions can take place via two main types of signaling: direct cell-to-cell contact and indirect cell-to-cell communication by secreting cytokines or exosomes [14]. Cytokines play important roles in mediating the crosstalk between different types of cells in the tumor microenvironment. To determine how G6PD activation in TNBC cells promoted M2-Mφ, the cytokine profile in the supernatants of MDA-231 cells with 6-AN treatment or G6PD knockdown was examined by cytokine array to identify the key factors in the communication between cancer cells and macrophage cells. The results indicated that CCL2 and TGF-β1 secretion was dramatically reduced in the supernatants after G6PD inhibition compared with the control (Fig. 3A). The *CCL2* and *TGF-β1* mRNA levels inhibited by G6PD downregulation were further detected by q-PCR (Fig. 3B). We also investigated the mRNA expression of other cytokines associated with M2-polarized macrophages in a cytokine array (Fig. 3C).

Next, ELISA confirmed that CCL2 and TGF-β1 secretion was promoted by G6PD overexpression in MCF10A cells and could be significantly repressed in TNBC cells with G6PD inhibition (Fig. 3D). To further confirm that CCL2 and TGF-β1 induced M2-like polarization, we added recombinant CCL2 and TGF-β1 to MDA-231 cell-CM after G6PD inhibition. Supplementation with either CCL2 or TGF-β1 effectively promoted CD163 and CD206 protein expression to induce M2-Mφ (Fig. 3E). In addition, the secretion of IL-10, a characteristic marker of M2-like TAMs, was also assessed. Consistent with alterations in immunoblotting, IL-10 secretion was higher in macrophages cocultured with CM supplemented with CCL2 or TGF-β1 (Fig. 3F). In brief, these findings implied that CCL2 and TGF-β1 secreted into the TME by TNBC cells could induce M2 polarization.

G6PD-controlled cytokine secretion achieved by STAT1 signaling

Then, we explored the signaling pathway of CCL2/TGF-β1 secretion regulated by G6PD. The STAT and NFκB signaling pathways are widely involved in macrophage polarization. In mammals, the JAK/STAT pathway is the main signaling mechanism for a wide array of growth factors and cytokines. Existing studies have confirmed aberrant STAT1 activation in breast cancer [15]. Meanwhile, the NFκB pathway plays an essential role in the regulation of immune responses and inflammation [16]. Hence, we analyzed the gene expression of *STAT1, STAT3 and RELA* in cancerous and noncancerous mammary tissues on the StarBase website (https://starbase.sysu.edu.cn/). *STAT1* gene expression was obviously increased in breast cancer tissue compared with normal breast tissue (Fig. 4A). To verify whether these signaling pathways are associated with CCL2/TGF-β1 secretion induced by G6PD, we examined the protein levels of STAT1/3 and NFκB in TNBC cells treated with 6-AN. Surprisingly, the expression of phospho-STAT3 did not appear to be altered in TNBC cells treated with 6-AN (Fig. S3A). Meanwhile, cells with G6PD knockdown increased the expression of phospho-NFκB (NFκB subunit p65) but decreased the expression of phospho-STAT1 in MDA-231 cells, and such tendency was also confirmed in MCF10A cells with G6PD overexpressing (Fig. 4B). Additionally, consistent with shRNA-mediated knockdown of G6PD, pharmacological inhibition of G6PD also resulted in decreased phospho-STAT1 and increased phospho-p65 in TNBC cells. However, the expression of G6PD showed no changes upon STAT1 inhibitor (fludarabine) and NFκB inhibitor (parthenolide) treatment (Figs. 4C and S3B). 6-AN significantly reduced the PPP flux and G6PD enzymatic activity without changing the G6PD protein and mRNA levels; likewise, the activity of G6PD showed no changes upon fludarabine and parthenolide treatment (Fig S3C-E). Finally, we evaluated whether STAT1 or NFκB signaling was involved in modulating the expression of G6PD-induced cytokines in TNBC cells. The mRNA levels of *CCL2* and

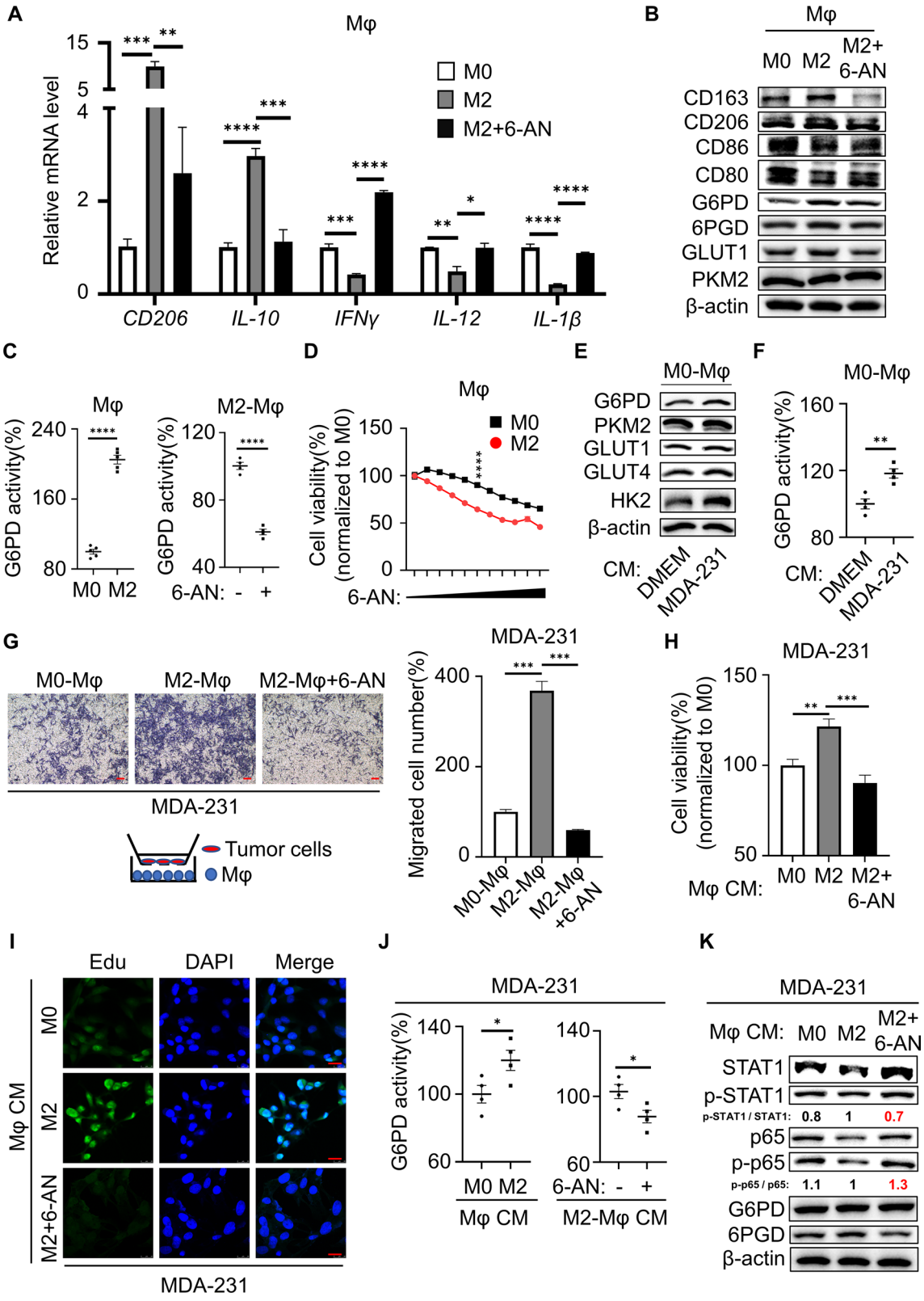

TGF-β1 were significantly decreased upon treatment with fludarabine, while parthenolide had a contradictory effect (Figs. S3F). Furthermore, ELISA showed that the secretion of CCL2 and TGF-β1 of MDA-231 cells had consistent mRNA results after fludarabine and parthenolide treatment (Fig. S3G). Next, we collected MDA-231-CM with

◂**Fig. 5** M2-Mφ synergized the malignant phenotype of TNBC via PPP. **A** The macrophages markers *CD206*, *IL-10*, *IL-12*, *IL-1β* and *IFNγ* were determined using q-PCR. **B** Protein expression in macrophages was examined using immunoblotting. **C** G6PD enzyme activity was detected in macrophages. **D** M0-Mφ and M2-Mφ were treated with different concentrations of 6-AN (0, 1.2, 2.4, 5, 10, 20, 40, 78, 156, 313 and 625 μM) for 48 h. Cell viability after drug treatment was measured using the MTT assay. **E** Altered proteins in M0-Mφ incubated with CM were measured by western blotting. **F** G6PD enzyme activity was detected in macrophages. **G** MDA-231 cells and macrophages were cocultured in the transwell migration experiment. Magnification 40×, bar = 200 μm. **H** The cell viability of MDA-231 cells cocultured with CM from macrophages for 48 h detected by MTT assay. **I** The proliferation of MDA-231 cells cocultured with CM from macrophages for 48 h detected by the EdU assay. The green color represents EdU positivity, and the blue color represents DAPI (nucleus). Representative images at 630× magnification is presented, bar = 25 μm. **J** G6PD enzyme activity was detected in MDA-231 cells coincubated with CM from macrophages. **K** Altered protein in MDA-231 cells incubated with the supernatant medium of macrophages was measured by western blot. **H–K** CM was transferred to MDA-231 cells after mixing 1:1 with fresh media. $^{*}P < 0.05$, $^{**}P < 0.01$, $^{***}P < 0.001$, $^{****}P < 0.0001$

different treatments and incubated with macrophages to observe changes in M2 polarization. The results showed that MDA-231-CM treated with parthenolide further induced M2 polarization, and there was a significant restraint in M2 polarization after G6PD knockdown in MDA-231 cells. On the anther hand, MDA-231-CM treated with fludarabine inhibited M2 polarization, and G6PD overexpression in MDA-231 cells induced M2 polarization (Fig. S3H).

We next investigated how G6PD orchestrated STAT1 signaling and NFκB signaling to regulate cytokine secretion and induce M2 polarization. The relevant literature showed that G6PD directly bound to certain proteins in the cells and induced downstream signaling pathway [17, 18]. Therefore, is there a direct contact between G6PD and STAT1 or NFκB(p65)? Interestingly, co-immunoprecipitation experiments showed that G6PD interacted with phospho-STAT1 in MDA-231 cells, rather than phospho-p65, p65 and STAT1 (Figs. 4D and S4A). Thus, we speculated that NFκB signaling changed might depend on the feedback effect formed by other indirect pathways. What's more, both 6-AN treatment and G6PD knockdown drastically reduced the quantity of protein through phospho-STAT1 pulling down by G6PD antibody in the same experiment condition (Fig. 4D). Furthermore, we examined whether G6PD and STAT1 regulation influences cytokine gene expression. It has been reported that IFNγ induced the activation of STAT1 signaling pathway [19], additional IFNγ promoted the expression of CCL2 and TGF-β1 after G6PD-knockdown (Figs. S4B and S4C). Analogously, we used siRNA to interfere with STAT1 and then overexpressed G6PD, results showed that CCL2 and TGF-β1 expression were activated in MDA-231 cells (Fig. S4D). The TIMER database and q-PCR further validated a positive correlation between G6PD and STAT1 in breast cancer (Figs. S4E and S4F). STAT1 belongs to the STAT protein family that form homo or hetero dimers and translocate to the nucleus to exert regulatory effects as a transcriptional activator [20]. To explore whether G6PD regulates phospho-STAT1 translocated into the nucleus, we separated the nucleus and cytoplasm of the cells. Lamin B1 and α-tubulin were used as markers of the nucleus and cytoplasm, respectively. As expected, STAT1 and phospho-STAT1 expression was inhibited in both nucleus and cytoplasm of cells with 6-AN treatment or G6PD knockdown (Fig. 4E). Naturally, we sought to identify whether CCL2 and TGF-β1 were regulated by STAT1. To this end, we queried the promoter sequence of CCL2 and TGF-β1 in the ensemble online website (https://asia.ensembl.org/index.html) to detect whether STAT1 could directly promote the transcription of CCL2 and TGF-β1. Potential binding site for STAT1 was discovered in the promoter region of CCL2 and TGF-β1 (Fig. 4F). The former and revised primers were designed around the potential binding motif, and the results of ChIP PCR illustrated that phospho-STAT1 could bind to the promoter region of CCL2 and TGF-β1 to promote its transcription, and the inhibition of G6PD further reduced the transcriptional expression of CCL2 and TGF-β1 (Fig. 4G,H and S5A). The TIMER database further validated a positive correlation between STAT1 and CCL2/TGF-β1 in breast cancer (Fig. S5B), which was consistent with our results. Overall, our study revealed that the STAT1 signaling pathway was involved in G6PD-regulated CCL2/TGF-β1 secretion.

M2-Mφ synergized the malignant phenotype of TNBC via PPP

The above results demonstrated the important role of G6PD in tumor cells, and in turn what effect did it have on macrophages? To this end, we inhibited/overexpressed G6PD in M0-Mφ cells. The results showed that M0-Mφ cells with G6PD silenced further suppressed M2 macrophage polarization and favoring M1 macrophage polarization, whereas M0-Mφ cells with G6PD-overexpressed possessing the opposite result (Figs. S6A and S6B). These results indicated a significant relationship between G6PD and macrophage polarization. During breast cancer progression, cancer cells interact with surrounding tissues to create a microenvironment. TAMs predominantly polarized toward M2-like macrophages and promoted malignant tumor progression. To investigate whether the antitumor effect of 6-AN also regulated M2-like macrophage polarization, we generated polarized M2-like macrophages. THP-1 cells were induced by PMA for 24 h and transformed into macrophages (M0-Mφ). Subsequently, IL-4 was administered to induce M2-Mφ differentiation. Firstly, we examined the change of the M2-type marker, and the results showed that the protein levels of

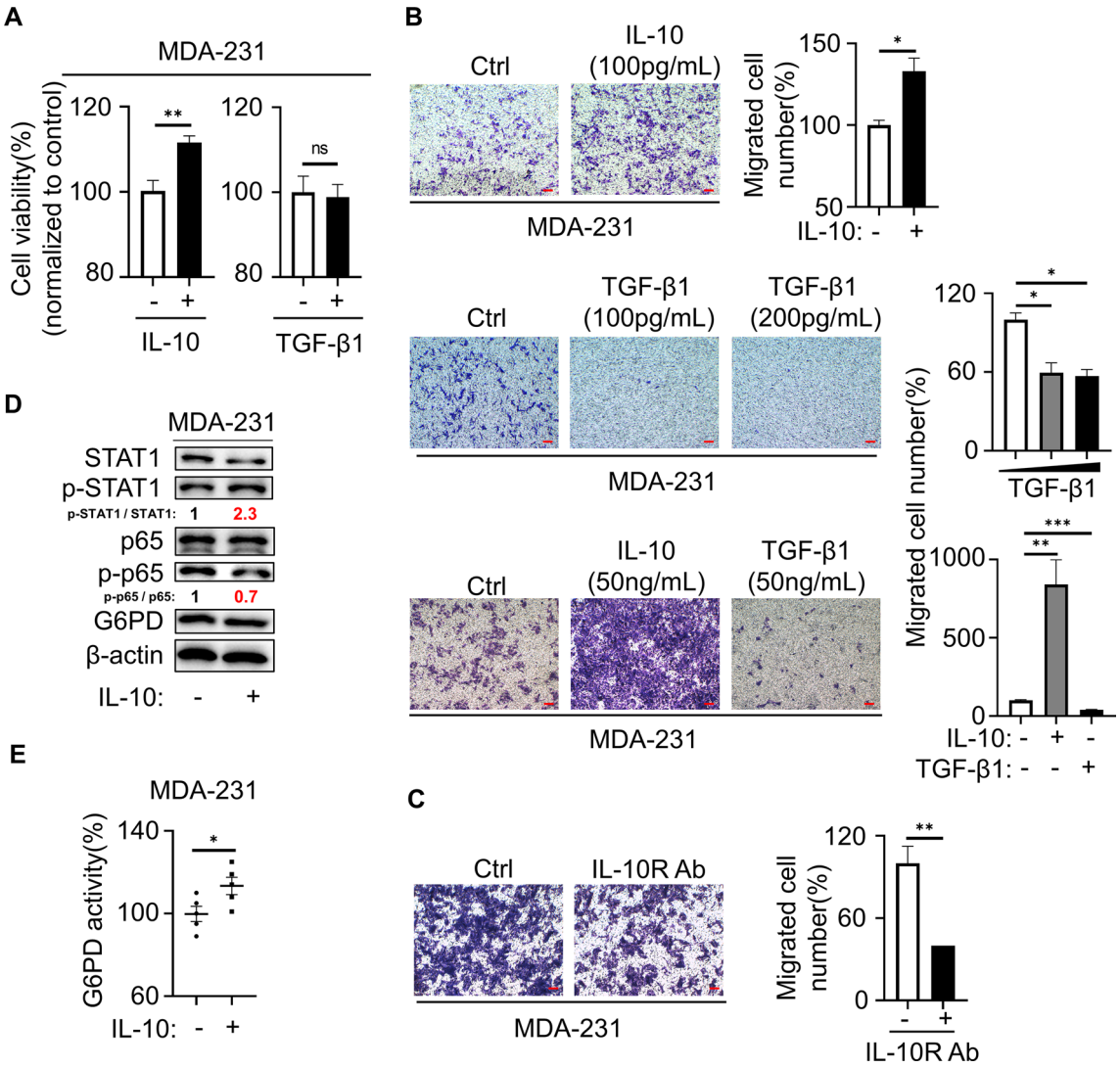

Fig. 6 M2-Mφ secretory IL-10 mediated PPP in TNBC. **A** MDA-231 cells were treated with 100 pg/mL IL-10 or TGF-β1 for 48 h, and cell viability was measured with MTT. **B** Cell migration was measured using transwell assays. Magnification 40×, bar = 200 μm. **C** Migration assays of MDA-231 cells were pretreated with IL-10R Ab (40 μg/mL) followed by IL-10 (200 pg/mL) coculture in the transwell for 48 h. Magnification 40×, bar = 200 μm. **D** Altered protein in MDA-231 cells that were treated with IL-10 (200 pg/mL) for 48 h was measured by western blot. **E** G6PD enzyme activity was detected in MDA-231 cells. $^{*}P < 0.05$, $^{**}P < 0.01$, $^{***}P < 0.001$

CD163 and CD206, the mRNA levels of *CD206* and *IL-10*, together with the secretion of IL-10 were all significantly increased in IL-4-stimulated macrophages (Fig. S6C–E), indicating that M2-Mφ were successfully induced by IL-4. In our study, we found that glucose metabolism, particularly the PPP, was activated in M2-Mφ compared with M0-Mφ, but the activation was counteracted by 6-AN (Fig. 5B, C, S6F and S6G). Interestingly, 6-AN treatment not only suppressed M2-Mφ polarization, but also switched macrophages from M2 to M1 (Figs. 5A,B and S6H). Moreover, compared with M0, 6-AN was more cytotoxic to M2-Mφ and suppressed its cell viability (Fig. 5D). The above results indicated that overactivation of the PPP is intrinsically required for tumor cells but is also essential for M2-Mφ. Further surveillance of macrophage glucose metabolism in cocultures with the CM of MDA-231 cells showed that the PPP was upregulated compared with DMEM (Fig. 5E, F). However, there was no significant change in PKM2, a key enzyme of glycolysis. Hence, our study revealed that macrophages were induced to become M2-Mφ in the TME of MDA-231 cells, accompanied by PPP activation. Meanwhile, we generated polarized M1-Mφ. The protein levels of CD86 and CD80, the mRNA levels of *CD86*, *IFNγ* and *IL-12*, and the secretion of IFNγ were significantly increased in LPS + IFNγ stimulated macrophages (Fig. S6I–K), indicating that M1-Mφ were successfully induced. Otherwise, both

the G6PD expression and activity were inhibited in M1–Mφ compared with M0–Mφ (Figs. S6I and S6L). To sum up, G6PD deficiency coordinately stimulated M1-Mφ conversion and inhibited M2-Mφ alternative activation, in which G6PD was downregulated in M1-Mφ but upregulated in M2. Therefore, 6-AN may be potential to inhibit M2 polarization and repolarization of M2 to M1-Mφ in the TME by targeting G6PD of macrophages to treat TNBC.

A previous study reported that M2-Mφ promoted breast cancer cell proliferation and migration in the tumor microenvironment [21]. To inspect whether migration and proliferation of TNBC cell are affected by M2-Mφ, the preconditioned macrophages were placed in the lower chamber to test the migration ability of MDA-231 cells from the upper chamber. The migration of MDA-231 cells was facilitated in coculturing with M2-Mφ, whereas pretreatment with 6-AN failed to activate M2 polarization, thus suppressing migration (Fig. 5G). Furthermore, MTT and EdU assays revealed that MDA-231 cells exhibited enhanced proliferation ability when incubated with the supernatants from M2-Mφ, while its proliferation was repressed by CM with 6-AN (Fig. 5H, I). Oncogene-driven metabolic reprogramming of cancer cells shapes the metabolism of neighboring cells and vice versa. Here, we wondered if M2-Mφ affected the PPP in MDA-231 cells. The supernatants of macrophages were collected and used as CM to culture MDA-231 cells, and the results showed that the supernatants from the M2-Mφ markedly promoted the PPP flow and the enzyme activity of G6PD in tumor cells (Figs. S6M, S6N and 5J). In addition, phospho-STAT1/STAT1 was significantly increased and phospho-p65/p65 was significantly decreased in MDA-231 cells, and these results were reversed by the G6PD inhibitor 6-AN (Fig. 5K), suggesting that the activation of G6PD in tumor cells might partially be attributed to M2-Mφ.

We demonstrated that TNBC cells influenced the polarization of macrophages through cytokines, and in turn whether macrophages influence tumor development through cytokines. M2-Mφ was reported to secrete growth factors, including IL-10 and TGF-β1, two of the most abundantly produced cytokines of TAMs [22]. To demonstrate that cytokines secreted by M2-Mφs involved in the proliferation and migration of TNBC, we directly added recombinant IL-10 or TGF-β1 to MDA-231 cells. The results indicated that cell migration and cell viability were significantly upregulated by IL-10 but not TGF-β1 (Fig. 6A,B). The enhanced migration of MDA-231 cells induced by the supernatants of IL-10 was abolished in the presence of the specific anti-IL-10 Ab (Fig. 6C). Similarly, MDA-231 cells treated with IL-10 further increased the glucose metabolism of breast cancer cells (Fig. 6D, E), suggesting that M2-Mφ might facilitate the PPP of TNBC cells through IL-10 secretion. A number of cytokines mediate their secretion through activation of the STAT and NFκB signaling pathways [23, 24]. In our study, the STAT1 and NFκB pathways were involved in the secretion of CCL2 and TGF-β1 in TNBC, and we assumed a similar mechanism in macrophages. Western blot results showed that the phospho-p65/p65 and phospho-STAT1/STAT1 ratios were increased, rather than phospho-STAT3/STAT3, during the process of M2 polarization, but the effect was restrained by 6-AN (Fig. S7A). To verify that IL-10 secretion was regulated by the STAT1 and NFκB pathways, we assessed the effects of the STAT1 inhibitor fludarabine or the NFκB inhibitor parthenolide in M2-Mφ. ELISA revealed that IL-10 secretion was markedly attenuated with fludarabine or parthenolide treatment, and the tendency was comparable to 6-AN (Fig. S7B). By Western blot, 6-AN treatment decreased the ratio of phospho-STAT1/STAT1 and phospho-p65/p65, but the G6PD level did not appear to be changed by parthenolide and fludarabine in M2-Mφ. Furthermore, CD163 and CD206 expression were decreased with all three kinds of inhibitors treatment (Fig. S7C and S7D). These results illustrated that the STAT1/NFκB signaling pathway might be involved in the regulation of M2 polarization of macrophages by G6PD. In addition, CCL2 or TGF-β1 supplementation alone was sufficient to activate the STAT1 and NFκB pathways in macrophages, as well as the CD163 and CD206 protein expression and mRNA levels of *CD206* and *IL-10*. Likewise, CD86 and IFNγ (M1 marker) showed no change under CCL2 and TGF-β1 stimulation (Figs. S7E and S7F). MDA-231 cells promoted survival when incubated with the supernatants from macrophages induced by CCL2, TGF-β1 or tumor cells CM (Fig. S7G). Therefore, these results suggested that M2-Mφ secreted IL-10 through PPP activation via the STAT1/NFκB pathway and promoted the PPP of TNBC cells to enhance their proliferation and migration ability.

Dual inhibition of M2-Mφ and TNBC cells by 6-AN in vivo

To investigate the influence of inhibiting G6PD on macrophage polarization and tumors in vivo, MDA-231 cells inoculated with M0 macrophages were subcutaneously transplanted into nude mice to establish a xenograft model. Tumor growth was monitored using a fluorescence imaging system and a Vernier caliper. The mean tumor fluorescence intensity in 6-AN-treated tumors was significantly decreased compared with that in the control group. Consistently, the tumor growth of the 6-AN group was also significantly inhibited (Fig. 7A). To further evaluate the inhibitory activity of 6-AN in vivo, tissue was collected for immunoblot and q-PCR analysis. The protein results showed that the M2-type macrophage markers CD163 and CD206 protein levels in the 6-AN group were significantly lower than those in the control group, the ratio of phospho-STAT1/STAT1

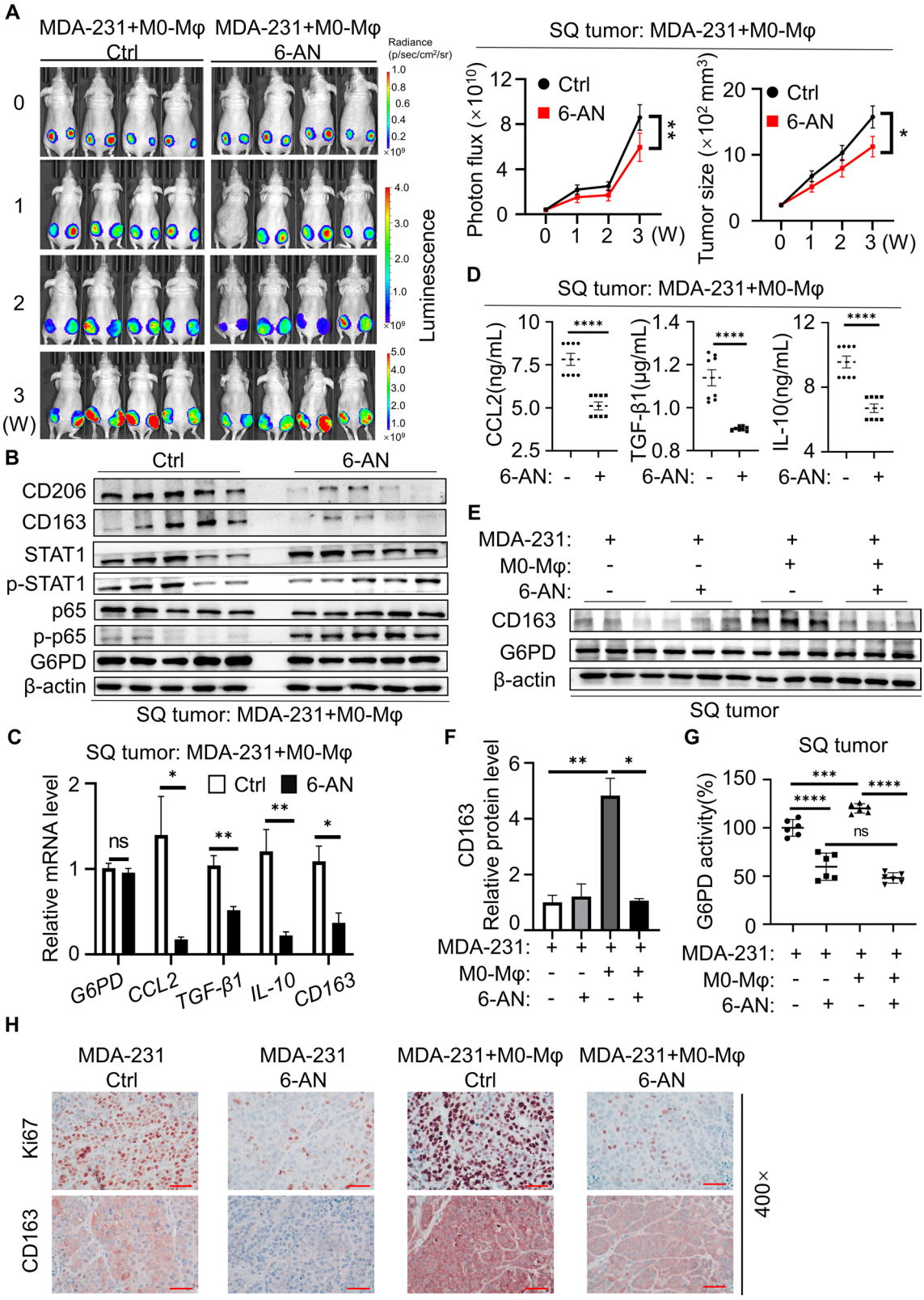
A
MDA-231+M0-Mφ Ctrl
MDA-231+M0-Mφ 6-AN
Radiance (p/sec/cm²/sr)
Luminescence
0
1
2
3 (W)
SQ tumor: MDA-231+M0-Mφ
Photon flux (×10¹⁰)
Tumor size (×10² mm³)
Ctrl
6-AN
(W)
B
Ctrl
6-AN
CD206
CD163
STAT1
p-STAT1
p65
p-p65
G6PD
β-actin
SQ tumor: MDA-231+M0-Mφ
C
SQ tumor: MDA-231+M0-Mφ
Relative mRNA level
ns
G6PD
CCL2
TGF-β1
IL-10
CD163
D
SQ tumor: MDA-231+M0-Mφ
CCL2(ng/mL)
TGF-β1(μg/mL)
IL-10(ng/mL)
6-AN:
E
MDA-231:
M0-Mφ:
6-AN:
CD163
G6PD
β-actin
SQ tumor
F
CD163 Relative protein level
MDA-231:
M0-Mφ:
6-AN:
G
SQ tumor
G6PD activity(%)
ns
H
MDA-231 Ctrl
MDA-231 6-AN
MDA-231+M0-Mφ Ctrl
MDA-231+M0-Mφ 6-AN
Ki67
CD163
400×

◂**Fig. 7** Dual inhibition of M2-Mφ and TNBC cells by 6-AN in vivo. **A** Tumor-bearing mice were intraperitoneally administered either vehicle or 6-AN (5 mg/kg, once every two days). The statistical graphs in the right panel indicate the photon flux of the tumor. Subcutaneous tumor size statistics after 20 days of mouse administration ($n=5$ in each group). **B** Immunoblot analysis of G6PD, STAT1, phospho-STAT1, p65, phospho-p65, CD163 and CD206 in xenograft tumors from mice treated with 6-AN. **C** The gene expression of *G6PD*, *CCL2*, *TGF-β1*, *IL-10* and *CD163* in xenograft tumor tissues was detected by q-PCR. **D** Cytokine levels in xenograft tumor tissues were determined by ELISA. **E** Immunoblotting was used to test G6PD and CD163 in xenograft tumors. **F** Densitometry was performed to analyze CD163 protein expression, and β-actin served as an internal reference. **G** G6PD enzyme activity was detected in xenograft tumors. **H** IHC staining for CD163 and Ki67 in orthotopic tumors. Magnification 400×, bar = 50 μm. $^{*}P<0.05$, $^{**}P<0.01$, $^{***}P<0.001$, $^{****}P<0.0001$

was decreased, and the ratio of phospho-p65/p65 was increased, revealing that STAT1 and NFκB pathway regulated by G6PD in tumor tissues were consistent with TNBC cells in vitro (Fig. 7B). In addition, 6-AN treatment significantly downregulated the mRNA expression of the cytokines *CCL2*, *TGF-β1* and *IL-10* in xenograft tumors (Fig. 7C). Additionally, ELISA was performed to detect the content of cytokines in tissue of all groups. 6-AN treatment was effective in decreasing the levels of the cytokines CCL2, TGF-β1 and IL-10 (Fig. 7D). In the TME, TAMs often exhibit M2 polarization and are associated with malignant transformation of tumor cells and poor prognosis of patients. Therefore, we detected whether macrophages exhibited M2 polarization in vivo by immunoblotting, and the protein results showed that CD163 was significantly increased in the MDA-231 plus M0-Mφ group, while CD163 expression was very low in the 6-AN treatment and MDA-231 groups (Fig. 7E, F). Meanwhile, the G6PD enzymatic activity of tumor tissue was detected, and it was found that compared with the MDA-231 group, the G6PD activity of the MDA-231 plus M0-Mφ group was increased. Similarly, 6-AN significantly reduced G6PD enzymatic activity without changing G6PD protein and mRNA expression (Fig. 7G). Finally, we checked CD163 and Ki67 expression in the primary tumor site by IHC staining. In the present study, the protein expression of the M2-Mφ markers CD163 and Ki67 in the 6-AN treatment group was significantly lower than that in the respective control group. Moreover, the expression levels of CD163 and Ki67 in the MDA-231 plus M0-Mφ group were significantly increased compared to those in the MDA-231 group alone (Fig. 7H). Taken together, these data suggested that the TNBC microenvironment induced the polarization of M2 macrophages to promote tumor proliferation. Moreover, 6-AN treatment inhibited xenograft tumor growth and macrophage M2 polarization in vivo.

Discussion

To date, TNBC is still the most intractable subtype of breast cancer. Several studies have identified extensive differences between the metabolic profiles of breast cancer and normal breast tissues, such as glycolysis, the pentose phosphate pathway, and amino acid, nucleotide and lipid metabolism [25–29]. Metabolic profiling also revealed high metabolic variability among different breast cancer cell lines. Lucas Willmann et al. analyzed metabolic differences in different breast cancer cells, and glycolysis in ER-positive cells was weaker than that in ER-negative cells [30], which was also proven in breast cancer tissues [31]. Metabolic changes in TNBC cells indicated increased energy demand, consistent with the aggressive biological behavior of the TNBC subtype [32]. In this study, we reported that G6PD in TNBC was overactivated. Given that G6PD is the first rate-limiting enzyme in the PPP, the activity of G6PD directly reflects the PPP flux. This result was consistent with the fact that the PPP played a critical role in regulating cancer cell growth by supplying cells with ribose-5-phosphate for ribose biogenesis and NADPH for intracellular ROS detoxification and reductive biosynthesis [33]. Furthermore, G6PD enhanced tumor growth by maintaining intracellular redox homeostasis. This could be the main reason why G6PD activity was increased in several types of cancers, including hepatoma, colorectal cancer, cervical carcinoma and bladder cancer [34–37]. These results underline the importance of G6PD in tumor development.

Recently, the cancer microenvironment was considered to be a complex system known as the TME, containing tumor cells, TAMs, interstitial cells, and noncellular components [38]. As an important component in the TME, TAMs interact with tumor cells and play pivotal roles in tumor progression by switching from the M1-like antitumor phenotype to the M2-like protumor phenotype [39, 40]. It is well established that TAMs (particularly M2-polarized TAMs) are key regulators of the therapeutic response in the TME [41]. M2-like TAMs promote angiogenesis, tumor migration and invasion, and are also associated with poor prognosis in breast cancer patients [42]. In this study, we identified G6PD overexpression in TNBC induced macrophage polarization toward an M2-like TAM phenotype, which in turn favored the activation of survival signaling that promoted proliferation and migration. Cytokines are canonical signals that directly link immune cells and tumor cells. The TME is enriched with cytokines that recruit circulating monocytes and favor the generation of TAMs resembling M2-type macrophages. We used a cytokine array to demonstrate that CCL2 and TGF-β1 were crucial secreted cytokines in G6PD mediating M2-like TAM polarization. To date, polarized activation

of macrophages has aroused extensive interest, and several main M2 stimuli has been identified, including CSF-1, IL4 and IL13 [43–45]. Our study suggested a significant role of CCL2 and TGF-β1 in M2-like TAM polarization in the tumor microenvironment of TNBC. STAT1, STAT3 and NFκB are important regulators of the production of inflammatory factors and the infiltration of inflammatory cells. Previous studies have demonstrated that the STAT signaling pathway plays an important role in oncogenesis mediated by G6PD [46]. G6PD deficiency regulates cytokine secretion by upregulating the NFκB pathway [47]. In other cell types, CCL2 and TGF-β1 expression is regulated by the NFκB- or STAT1-mediated signaling pathway or directly bound to their promoter region [48–51]. Additionally, the elevation of CCL2 evoked aggressive forms of malignant tumors characterized by TAM recruitment, cell proliferation, invasion and angiogenesis. We obtained similar results showing that TGF-β1 contributed to M2 macrophage polarization [52]. In our research, we found that phospho-STAT1(Ser727) and G6PD could be directly combined and initially identified STAT1 signaling–dependent cytokine secretion in TNBC, which contributed to M2-like macrophage activation.

It is well known that macrophages have divided loyalties and can change their functions in response to the TME. During the process of inflammation, macrophages adopt distinct metabolic signatures as they switch from quiescent to activated states. However, the importance of metabolic crosstalk in tumor immunity and progression and the mechanism for regulating glucose metabolism in TAMs are poorly understood. Emerging evidence suggests that glycolysis promotes proinflammatory effects in macrophages; simultaneously, it is also crucial for M2 subtype macrophage activation [53]. Our current data suggested that the PPP was activated rather than glycolysis in M2-Mφ. Interestingly, in addition to inhibiting TNBC, we further discovered that 6-AN restrained M2 transformation and viability. Moreover, our results suggested that STAT1 and NFκB signaling was activated in M2-Mφ induced by IL-4 or cocultured with MDA-231 cells, thus upregulating IL-10 secretion in macrophages. TAMs have the property of M2-Mφ, which are related to cancer progression, and the role of M2-like TAMs in promoting tumor growth and migration has been widely investigated [54]. Similar to many other immune cells, macrophages can rapidly adjust their cellular metabolism in response to the TME, and TAMs, in turn, regulate the biological behavior of tumor cells by secreting small molecular substances. IL-10 and TGF-β1 are the most abundantly produced cytokines in TAMs. Our results indicated that migration and cell viability were significantly promoted by IL-10 but not TGF-β1. TGF-β1 can be tumor promoted or suppressive. The effects of TGF-β1 depended on the cellular context, and this contextual nature was particularly manifested in tumors. In cancer cell lines with high autocrine TGF-β production, endogenous TGF-β1 opposed the migratory and growth-inhibitory responses induced by MEK-ERK signaling [55]. Apoptosis in TGF-β-sensitive PDA cells is induced by TGF-β [56]. Similarly, our research revealed that TGF-β1 inhibited the migration of MDA-231 cells but had no effect on proliferation. Furthermore, our findings suggested that M2-like macrophages substantially activated the PPP of MDA-231 cells, which further accelerated the process of migration and proliferation in TNBC. In addition, studies have shown that tumor-derived cytokines induce the polarization of M2 macrophages and promote tumor progression in a xenograft nude murine model [57, 58]. This was also consistent with our in vivo experiments. G6PD-overexpressing TNBC tissues were infiltrated with more M2-like TAMs. The downregulation of G6PD activity by 6-AN in TNBC cancer cells led to decreased tumorigenesis accompanied with expression suppression of M2-polarizing markers such as CD163, CD206, TGF-β1 and IL-10. Under the premise of reprogramming glucose metabolism, the crosstalk between TNBC and macrophages via cytokines forms a loop to jointly promote tumor progression.

However, there are some disadvantages in this study. We did not fully examine the molecular mechanism of the signaling pathway in macrophages, and we will further identify it in the future. In addition, our data preliminarily suggested that G6PD participated and affected the polarization of macrophages, and that G6PD directly bound to phospho-STAT1 (Ser727) to regulate cytokine secretion and macrophage polarization. While phospho-STAT1 (Tyr701) and G6PD did not interact with each other in Co-IP experiments (results not shown), it is not enough to explain the mechanism, and more in-depth future studies required to clarify. Based on these findings, we considered a better understanding of the circuits between TAMs and TNBC to facilitate TNBC diagnosis, prevention and therapeutics.

Conclusion

In summary, our data shed light on an important role of the feedback circuit between G6PD overexpression in TNBC and macrophage polarization in TNBC progression, thus providing new insights and robust preclinical evidence for targeting G6PD in the treatment of TNBC.

Supplementary Information The online version contains supplementary material available at https://doi.org/10.1007/s00018-023-04810-y.

Acknowledgements We would like to thank Gang Zhao (Department of Pathology, Tianjin Cancer Hospital) and the breast surgery department of Peking Union Medical College Hospital for supplying breast

cancer tissue sections, Miaomiao Sheng (Kunming University of Science and Technology) for providing breast cancer cell lines, and Xinying Wu (Animal Center of Nankai University) for technical support of in vivo imaging.

Author contributions Y L, X H and Z F designed, performed and analyzed the in vivo experiments. Y L, X H and Z F performed and analyzed G6PD knockdown experiments in vitro and in vivo. Y L, X H and Z L provided guidance on data processing and writing. C L, Y L, C W, Q S and Z F contributed to the study design, implementation and supervision of the study. Z L, Z F, C W, Q S and C L contributed to the study design, supervised the study, and reviewed the manuscript. Y L and C L wrote the manuscript. All authors had full access to the data and approved the final version of the manuscript.

Funding This study was partially funded by "State Key Laboratory of Medicinal Chemical Biology (NanKai University, No. 2019014)" to C W and "The Fundamental Research Funds for the Central Universities (Nankai University, #ZB19100128)" to C L.

Data availability The authors confirm that the data supporting the findings of this study are available within the article. The raw data are available from the corresponding author upon reasonable request. Figure 1D data analyzed in this study were obtained from the Gene Expression Omnibus (GEO) at GSE81032.

Declarations

Conflict of interests The authors declare that they have no competing interests.

Ethics approval and consent to participate Animal experiments were performed according to the Guidelines on Laboratory Animals of Nankai University and were approved by the Institute Research Ethics Committee at Nankai University (No: 2021-SYDWLL-000464). Human experiments were approved by the human experimentation committee, and informed consent was obtained from all subjects (No: NKUIRB2021105).

Consent for publication Not applicable.

References

1. Siegel RL et al (2021) Cancer Statistics, 2021. CA Cancer J Clin 71(1):7–33
2. Yin L et al (2020) Triple-negative breast cancer molecular subtyping and treatment progress. Breast Cancer Res 22(1):61
3. Robey IF et al (2005) Hypoxia-inducible factor-1alpha and the glycolytic phenotype in tumors. Neoplasia 7(4):324–330
4. Pu H et al (2015) Overexpression of G6PD is associated with high risks of recurrent metastasis and poor progression-free survival in primary breast carcinoma. World J Surg Oncol 13:323
5. Dong T et al (2016) Altered glycometabolism affects both clinical features and prognosis of triple-negative and neoadjuvant chemotherapy-treated breast cancer. Tumour Biol 37(6):8159–8168
6. Tu D et al (2021) M2 macrophages contribute to cell proliferation and migration of breast cancer. Cell Biol Int 45(4):831–838
7. Jayasingam SD et al (2019) Evaluating the polarization of tumor-associated macrophages into m1 and m2 phenotypes in human cancer tissue: technicalities and challenges in routine clinical practice. Front Oncol 9:1512
8. Chen P et al (2017) Gpr132 sensing of lactate mediates tumor-macrophage interplay to promote breast cancer metastasis. Proc Natl Acad Sci USA 114(3):580–585
9. Chen F et al (2019) Extracellular vesicle-packaged HIF-1alpha-stabilizing lncRNA from tumour-associated macrophages regulates aerobic glycolysis of breast cancer cells. Nat Cell Biol 21(4):498–510
10. Li Y et al. (2022) Targeting glucose-6-phosphate dehydrogenase by 6-AN induces ROS-mediated autophagic cell death in breast cancer. FEBS J.
11. Shi T et al. Conservation of protein abundance patterns reveals the regulatory architecture of the EGFR-MAPK pathway. Sci Signal, 2016. **9**(436): p. rs6.
12. Dias AS et al (2019) Metabolic crosstalk in the breast cancer microenvironment. Eur J Cancer 121:154–171
13. Zheng H et al. (2021) Tumor Microenvironment: Key Players in Triple Negative Breast Cancer Immunomodulation. Cancers (Basel) 13(13).
14. Nishida-Aoki N, Gujral TS (2019) Emerging approaches to study cell-cell interactions in tumor microenvironment. Oncotarget 10(7):785–797
15. Tymoszuk P et al (2014) High STAT1 mRNA levels but not its tyrosine phosphorylation are associated with macrophage infiltration and bad prognosis in breast cancer. BMC Cancer 14:257
16. Tilborghs S et al (2017) The role of Nuclear Factor-kappa B signaling in human cervical cancer. Crit Rev Oncol Hematol 120:141–150
17. Ma X et al (2017) Polo-like kinase 1 coordinates biosynthesis during cell cycle progression by directly activating pentose phosphate pathway. Nat Commun 8(1):1506
18. Ni Y et al (2021) Silent information regulator 2 promotes clear cell renal cell carcinoma progression through deacetylation and small ubiquitin-related modifier 1 modification of glucose 6-phosphate dehydrogenase. Cancer Sci 112(10):4075–4086
19. Butturini E, Carcereri de Prati A, Mariotto S (2020) Redox Regulation of STAT1 and STAT3 Signaling. Int J Mol Sci. 21(19).
20. Verhoeven Y et al (2020) The potential and controversy of targeting STAT family members in cancer. Semin Cancer Biol 60:41–56
21. Ch'ng ES, Jaafar H (2011) Tuan Sharif SE Breast Tumor Angiogenesis and Tumor-Associated Macrophages: Histopathologist's Perspective. Patholog Res Int. 2011: 572706.
22. Wang H, et al. (2021) The impact of the tumor microenvironment on macrophage polarization in cancer metastatic progression. Int J Mol Sci. 22(12).
23. Owen KL, Brockwell NK, Parker BS (2019) JAK-STAT Signaling: A Double-Edged Sword of Immune Regulation and Cancer Progression. Cancers (Basel). 11(12).
24. Sun SC (2017) The non-canonical NF-kappaB pathway in immunity and inflammation. Nat Rev Immunol 17(9):545–558
25. Sun L et al (2018) Metabolic reprogramming for cancer cells and their microenvironment: beyond the Warburg Effect. Biochim Biophys Acta Rev Cancer 1870(1):51–66
26. Jiang P, Du W, Wu M (2014) Regulation of the pentose phosphate pathway in cancer. Protein Cell 5(8):592–602
27. More TH et al (2018) Metabolomic alterations in invasive ductal carcinoma of breast: a comprehensive metabolomic study using tissue and serum samples. Oncotarget 9(2):2678–2696
28. Tayyari F et al (2018) Metabolic profiles of triple-negative and luminal A breast cancer subtypes in African-American identify key metabolic differences. Oncotarget 9(14):11677–11690
29. Budczies J et al (2012) Remodeling of central metabolism in invasive breast cancer compared to normal breast tissue—a GC-TOFMS based metabolomics study. BMC Genomics 13:334
30. Willmann L et al (2015) Metabolic profiling of breast cancer: differences in central metabolism between subtypes of breast

cancer cell lines. J Chromatogr B Analyt Technol Biomed Life Sci 1000:95–104
31. Tang X et al (2014) A joint analysis of metabolomics and genetics of breast cancer. Breast Cancer Res 16(4):415
32. Willmann L et al (2016) Alterations of the exo- and endometabolite profiles in breast cancer cell lines: a mass spectrometry-based metabolomics approach. Anal Chim Acta 925:34–42
33. Patra KC, Hay N (2014) The pentose phosphate pathway and cancer. Trends Biochem Sci 39(8):347–354
34. Yin X et al (2017) ID1 promotes hepatocellular carcinoma proliferation and confers chemoresistance to oxaliplatin by activating pentose phosphate pathway. J Exp Clin Cancer Res 36(1):166
35. Barajas JM et al (2018) The role of miR-122 in the dysregulation of glucose-6-phosphate dehydrogenase (G6PD) expression in hepatocellular cancer. Sci Rep 8(1):9105
36. Wu S et al (2018) Transcription factor YY1 promotes cell proliferation by directly activating the pentose phosphate pathway. Cancer Res 78(16):4549–4562
37. Massari F et al (2016) Metabolic phenotype of bladder cancer. Cancer Treat Rev 45:46–57
38. Pathria P, Louis TL, Varner JA (2019) Targeting tumor-associated macrophages in cancer. Trends Immunol 40(4):310–327
39. Mantovani A et al (2017) Tumour-associated macrophages as treatment targets in oncology. Nat Rev Clin Oncol 14(7):399–416
40. Cook J, Hagemann T (2013) Tumour-associated macrophages and cancer. Curr Opin Pharmacol 13(4):595–601
41. Pitt JM et al (2016) Targeting the tumor microenvironment: removing obstruction to anticancer immune responses and immunotherapy. Ann Oncol 27(8):1482–1492
42. Castellaro AM et al. (2019) Tumor-associated macrophages induce endocrine therapy resistance in ER+ breast cancer cells. Cancers (Basel). 11(2).
43. Munoz-Garcia J et al (2021) The twin cytokines interleukin-34 and CSF-1: masterful conductors of macrophage homeostasis. Theranostics 11(4):1568–1593
44. Sica A, Mantovani A (2012) Macrophage plasticity and polarization: in vivo veritas. J Clin Invest 122(3):787–795
45. Shapouri-Moghaddam A et al (2018) Macrophage plasticity, polarization, and function in health and disease. J Cell Physiol 233(9):6425–6440
46. Hu T et al (2013) Variant G6PD levels promote tumor cell proliferation or apoptosis via the STAT3/5 pathway in the human melanoma xenograft mouse model. BMC Cancer 13:251
47. Yang HC et al (2015) Glucose 6-phosphate dehydrogenase knockdown enhances IL-8 expression in HepG2 cells via oxidative stress and NF-kappaB signaling pathway. J Inflamm (Lond) 12:34
48. Dai L et al (2019) SARI attenuates colon inflammation by promoting STAT1 degradation in intestinal epithelial cells. Mucosal Immunol 12(5):1130–1140
49. Jia P et al. (2022) Chemokine CCL2 from proximal tubular epithelial cells contributes to sepsis-induced acute kidney injury. Am J Physiol Renal Physiol.
50. Cao J et al (2021) NR4A1 knockdown confers hepatoprotection against ischaemia-reperfusion injury by suppressing TGFbeta1 via inhibition of CYR61/NF-kappaB in mouse hepatocytes. J Cell Mol Med 25(11):5099–5112
51. Duke KS et al (2017) STAT1-dependent and -independent pulmonary allergic and fibrogenic responses in mice after exposure to tangled versus rod-like multi-walled carbon nanotubes. Part Fibre Toxicol 14(1):26
52. Zhang F et al (2016) TGF-beta induces M2-like macrophage polarization via SNAIL-mediated suppression of a pro-inflammatory phenotype. Oncotarget 7(32):52294–52306
53. Van den Bossche J, O'Neill LA, Menon D (2017) Macrophage Immunometabolism: Where Are We (Going)? Trends Immunol 38(6):395–406
54. Noy R, Pollard JW (2014) Tumor-associated macrophages: from mechanisms to therapy. Immunity 41(1):49–61
55. Ungefroren H et al. (2021) Autocrine TGFbeta1 opposes exogenous tgfbeta1-induced cell migration and growth arrest through sustainment of a feed-forward loop involving MEK-ERK signaling. Cancers (Basel), 13(6).
56. David CJ et al (2016) TGF-beta tumor suppression through a Lethal EMT. Cell 164(5):1015–1030
57. Chen RH et al (2020) Tumor cell-secreted ISG15 promotes tumor cell migration and immune suppression by inducing the macrophage M2-like phenotype. Front Immunol 11:594775
58. Su B et al (2021) Let-7d inhibits intratumoral macrophage M2 polarization and subsequent tumor angiogenesis by targeting IL-13 and IL-10. Cancer Immunol Immunother 70(6):1619–1634